Dalton Transactions

COMMUNICATION

View Article Online
View Journal | View Issue

Cite this: *Dalton Trans.*, 2014, **43**, 17904

Received 14th August 2014,
Accepted 18th September 2014

DOI: 10.1039/c4dt02476a

www.rsc.org/dalton

Controlled synthesis and characterization of the elusive thiolated Ag_{55} cluster†

Indranath Chakraborty,[a] Shrabani Mahata,[b] Anuradha Mitra,[c] Goutam De[c] and Thalappil Pradeep*[a]

A stable, Ag_{55} cluster protected with 4-(*tert*-butyl)benzyl mercaptan (BBSH) was synthesized which exhibits two prominent absorption bands with maxima at 2.25 and 2.81 eV. A molecular ion peak at *m/z* 11 500 ± 20 in matrix assisted laser desorption ionization mass spectrum (MALDI MS), assigned to $Ag_{55}(BBS)_{31}$ was observed. Electrospray ionization (ESI MS) shows a prominent trication along with higher charged species. An analogous $Ag_{55}(PET)_{31}$ (PET = 2-phenylethanethiol, in the thiolate form) was also synthesized under optimized conditions which proves the amenability of this cluster and the synthetic methodology to other ligands.

Monolayer protected noble metal quantum clusters (QCs) composed of few atoms are completely different from their corresponding bulk analogues.[1–3] Due to their unique optical and luminescent properties, they have been applied in diverse applications such as sensing,[4–6] catalysis,[7,8] antibacterial,[9] drug delivery,[10] *etc.* Stable QCs satisfy the criteria of either geometric (*e.g.* Au_{13},[11] Au_{55},[12] *etc.*) or electronic (*e.g.* $Au_{11}(PH_3)_7(SMe)$,[13] $Au_{25}SR_{18}$,[14,15] $Au_{102}(SR)_{44}$,[16] *etc.*) closed shells; the latter may form by ionic cores as well. Among such stable clusters, $Au_{55}(PR_3)_{12}Cl_6$ is an early example.[17] Inertness of the Au_{55} nucleus, ability to make bare clusters[18] and crystals,[19] observation of phenomena such as single-electron tunneling[20] and interactions with several bio-systems[21] made this cluster interesting. Recently, new methods have been developed to synthesize thiol protected Au_{55} in the organic phase which facilitated further characterization.[22–25] Although several QCs of silver with known chemical composition such as water soluble Ag_7,[26] $Ag_{7,8}$,[27] and Ag_9,[28] as well as organic soluble Ag_{44},[29,30] Ag_{140},[31] Ag_{152},[32] and Ag_{280} [33] have been made and crystal structures of Ag_{14},[34] Ag_{16},[35] Ag_{32} [35] and Ag_{44} [36,37] have been reported, the growth of the area is not comparable to that of gold analogues.[1,14,16,24,38–40] This is especially noticeable from the absence of reports of clusters of the kind, Ag_{13} and Ag_{55} for which the gold counterparts have been known since 1981. Recently, we have shown the optical spectrum of the 2-phenylethanethiol protected Ag_{55} cluster while exploring the appearance of plasmon excitation in silver clusters.[41]

Here, we report thiolated Ag_{55} clusters and their most essential characterization. The synthesis involves reaction of the metal salt ($AgNO_3$) and the thiol (BBSH) in a 1 : 4 ratio in a mortar and pestle to form the thiolate in the solid state. Addition of $NaBH_4$ powder under the laboratory atmosphere and continued grinding makes the clusters which are extracted with toluene, to give a crude sample. The toluene extract was precipitated by MeOH and re-extracted in toluene which results in the purified cluster sample. The cluster is stable for 8 days in solution under ambient conditions. The stability enhances under reduced temperatures. A powder sample is stable for extended periods (additional information is given in ESI 1†).

MALDI MS analyses (all experimental details are given in ESI 1†) were done on crude (red trace in Fig. 1) and purified (black trace in Fig. 1) clusters using *trans*-2-[3-(4-*tert*-butylphenyl)-2-methyl-2-propenylidene]malononitrile (DCTB) as the matrix which is known to be ideal for organic thiol-protected metal nanoclusters.[41,42] Threshold laser power (f_{th}) was used to detect the molecular ion peak without fragmentation. For both the cases, molecular ion peak at *m/z* 11 500 ± 20 (the uncertainty is largely due to the isotope distribution and also due to inherent instrumental limitations) was seen and was assigned as $Ag_{55}(BBS)_{31}$ (expected mass: 11 510). Even though the peak maximum was the same for the purified and crude cluster samples, there was a difference in peak width between the two. The purified cluster has a full width at half maximum (FWHM) of 3.3 kDa whereas it is 5.5 kDa for the crude cluster. This increased width may be due to the presence of extra thiols or thiolates in the crude cluster which is responsible for peak broadening. FWHM of silver clusters are broad in nature compared to gold clusters and we have studied them extensively.[41] Laser intensity-dependent study (Fig. S2, ESI†) shows

[a]*DST Unit of Nanoscience (DST UNS) and Thematic Unit of Excellence, Department of Chemistry, Indian Institute of Technology Madras, Chennai 600 036, India. E-mail: pradeep@iitm.ac.in; Fax: +91-44 2257-0545*
[b]*National Institute of Science and Technology, Berhampur, Odisha, India*
[c]*CSIR-Central Glass and Ceramics Research Institute, Kolkata, India*

† Electronic supplementary information (ESI) available: Details of experimental procedures and characterization using ESI MS, XPS, SEM/EDAX, XRD of $Ag_{55}(BBS)_{31}$ clusters. See DOI: 10.1039/c4dt02476a

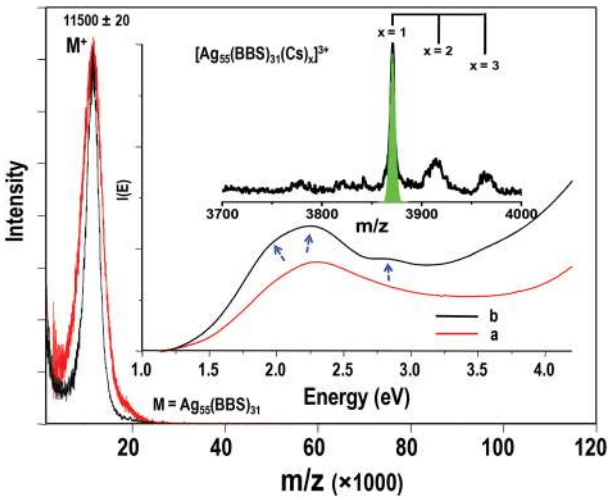

Fig. 1 MS spectra of the as-synthesized crude cluster (red trace) and the purified Ag_{55} cluster (black trace). Inset shows the UV/Vis spectra for the same (a: the crude cluster, b: purified cluster) plotted as a function of energy. Jacobian-corrected intensities are plotted (details are given in ESI†). The purified cluster shows two prominent bands at 2.25 and 2.81 eV and a weak band at 1.93 eV (marked) whereas the crude one shows only a broad band at 2.28 eV. Inset of inset shows the ESI† mass spectrum of the purified cluster (in positive mode) which shows a prominent peak at *m*/*z* 3870 corresponding to $[Ag_{55}(BBS)_{31}Cs]^{3+}$. The corresponding calculated isotope distribution is shown in green.

similar observation as reported in the case of $Ag_{152}(PET)_{60}$.[42] With increase in laser fluence, $f = xf_{th}$, $x > 1.02$, a systematic mass loss was observed till $x = 1.37$. No further loss was seen after that. Like the Ag_{152} cluster,[42] a similar sharp rise at the low mass side and steep fall at the high mass side was seen when laser fluence was varied. Significant difference was also observed in the optical spectra (inset of Fig. 1) for both the clusters. The crude cluster shows a broad feature at 2.28 eV (543 nm) whereas the purified cluster shows two prominent bands at 2.25 eV (550 nm) and 2.81 eV (440 nm) along with a week band at 1.93 eV (640 nm). The prominent step-like feature and absence of plasmon (seen in nanoparticle) confirmed the formation of a molecular species.

ESI MS is an ideal tool to determine the precise composition of nanoclusters.[25,27,28,43] As BBSH is completely non-polar, cesium acetate (CsOAc) was used to ionize the molecule. The cluster solution was taken in a toluene–methanol mixture and the spectra (Fig. S3, ESI†) were collected in the *m*/*z* range of 200–4000 (maximum limit of the instrument). A prominent peak at *m*/*z* 3870 (inset of Fig. 2) corresponding to $[Ag_{55}(BBS)_{31}Cs]^{3+}$ which matches exactly with the calculated spectrum (green trace) was observed. The two isotopes of silver, namely, 107 and 109, with equal natural abundances and the isotopes of carbon and sulfur together make the overall cluster peak too complex and specific peaks were not resolved for this charge state. However, the spectral envelope was reproduced clearly and was identical to the calculated spectrum. Systematic Cs addition to this peak was also observed. As the peaks are due to 3+ charge, the peak separation was 133/3 = 44.3, which is marked in the figure. This type of Cs induced ionization and corresponding Cs addition peaks have been reported for the $Au_{333}(SCH_2CH_2Ph)_{79}$ cluster.[44] The composition was further supported by the presence of $[Ag_{55}(BBS)_{31}Cs_4]^{4+}$, $[Ag_{55}(BBS)_{31}Cs_5]^{5+}$ and $[Ag_{55}(BBS)_{31}Cs_6]^{6+}$ at *m*/*z* 3005, 2431 and 2048, respectively (Fig. S3, ESI†), although these peaks are not prominent. It is important to recall that well-defined mass spectra of this kind are rare in the case of silver clusters (except for the Ag_{44} cluster which shows distinct mass spectral features). We could not see the 4+, 5+ or 6+ ions of $[Ag_{55}(BBS)_{31}]$ without Cs. This is probably due to the fact that the cluster is inefficient to take these many charges on its own. Some fragments were also seen in the spectrum and few of them have been identified. The highest intense pattern is expanded in the inset of Fig. S3, ESI† which shows a precise isotope distribution. It matches exactly with the calculated spectrum of $[Ag_5(BBS)_6Cs_2]^+$. Although the unit charge on a Cs_2-bound species is surprising, it may be noted that $Ag_5(BBS)_6$ is likely to be an anion due to an excess BBS ligand and therefore, $[Ag_5(BBS)_6Cs_2]$ is a singly charged cation. These types of fragments are most stable which explains their high intensity. Even under softer ionizing conditions, the fragment intensity has not been reduced.

TG analysis of the $Ag_{55}(BBS)_{31}$ cluster shows a weight loss of 47.9 ± 0.5% which corresponds to the total organic content of the material (Fig. 2A). The calculated organic content of the cluster is 48.5% which matches with the experimental results further supports the composition. Interestingly, two kinds of losses were seen, one at 200 °C (42.30%) and another at 800 °C (5.58%). The major loss may be due to the carbon–hydrogen (CH) content of the ligand which happens at a lower temperature and the remaining fragment of the ligand, namely sulfur which sits on the metal surface to form a nearly stoichiometric Ag_2S and the sulfur leaves at higher temperature. This kind of

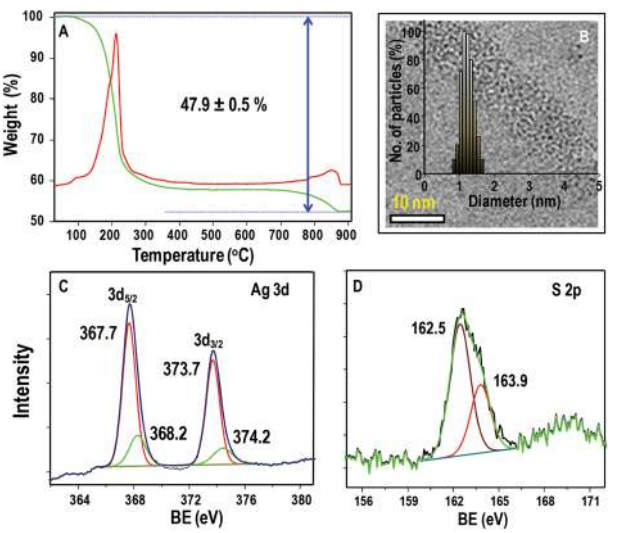

Fig. 2 TGA spectrum of the Ag_{55} cluster (green trace) which shows two types of weight losses (A). Red trace is a differential plot of the same. 'B' shows the TEM image of the Ag_{55} cluster and inset is the corresponding size distribution curve. 'C' and 'D' are the extended XPS spectra for Ag 3d and S 2p regions. All the spectra are properly fitted.

sulfide formation is consistent with the solution phase decomposition of thiolated silver clusters reported previously[45] where facile C–S cleavage occurs, facilitating the formation of Ag_2S in the acanthite form.

PXRD analysis (Fig. S4, ESI†) of the $Ag_{55}(BBS)_{31}$ cluster powder in the 2θ range of 10° to 90° showed broad diffraction peaks at $2\theta \sim 37°$, 44° and 64°. Individual silver clusters do not contain a periodic lattice in them and so they do not show sharp peaks. However, the broad lines are observed.[28] The $Ag_{55}BBS_{31}$ composition was further verified with SEM/EDAX data (Fig. S5, ESI†) where the Ag : S ratio was found as 1 : 0.61 ± 0.05 (calculated value 1 : 0.57). The absence of sodium in the EDAX spectrum confirms the purity of the cluster. The TEM image (Fig. 2B) shows the presence of the cluster as tiny particles with an average size (diameter) of 1.15 nm. Bigger sized nanoparticles were not seen. XPS analysis was performed to know the chemical states of elements, although there is not much difference (only 0.5 eV) in the binding energies of Ag(0) and Ag(I).[46] A survey spectrum (Fig. S6, ESI†) shows the expected elements. Expanded spectra of Ag 3d (Fig. 2C) show the presence of Ag(0) and a small portion of Ag(I) which might be coming from the thiolate shell. The S 2p peak at 162.5 eV (corresponding to $2p_{3/2}$) is because of thiolate (Fig. 2D).

FTIR spectra of BBSH and $Ag_{55}(BBS)_{31}$ are given in Fig. 3A. The spectrum of BBSH shows characteristic stretching and bending modes of various bonds present in it. The absence of S–H stretching at 2585 cm^{-1} in the Ag_{55} cluster confirms the binding of thiol to the silver core. Interesting difference was found between the cluster and BBSH in the C–H stretching (Fig. 3B) and bending regions (Fig. 3C). Intensities of the 3063 and 3086 cm^{-1} peaks in the C–H stretching region (of $-CH_2-$) decrease and show a red shift when the thiol binds to the cluster which suggests that this C–H part of the ligand is

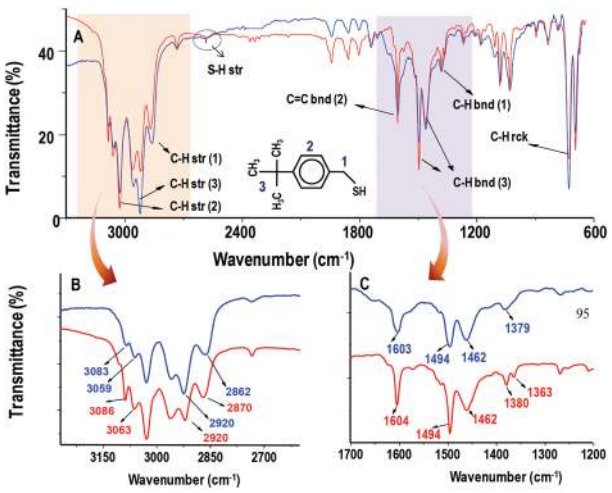

Fig. 3 (A) FT-IR spectra of pure BBSH (blue trace) and $Ag_{55}(BBS)_{31}$ cluster (red trace). The –SH stretching featured at 2586 cm^{-1} in BBSH is marked by a dotted-circle which is absent in the cluster. The structure of BBSH is shown as an inset in which different IR-active parts are numbered. The expanded views of C–H stretching and bending regions are given as (B) and (C), respectively. For clarity, the spectra have been shifted slightly.

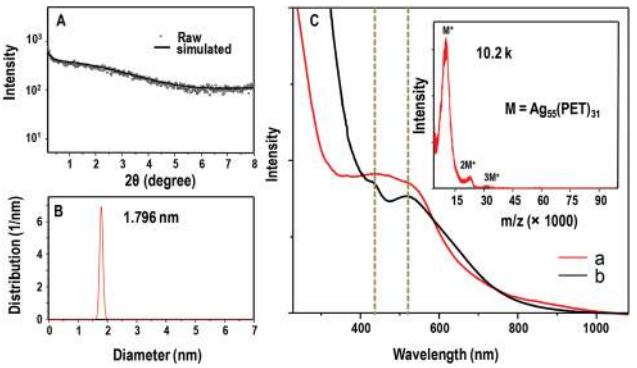

Fig. 4 SAXS analysis of the Ag_{55} cluster. Experimental and simulated (nonlinear least squares method) SAXS curves are shown in the top (A) and the corresponding particle size distribution obtained from the SAXS profile is shown in the bottom panel (B). UV/Vis spectra of the $Ag_{55}(BBS)_{31}$ cluster compared with the PET protected Ag_{55} cluster (C). Inset is the MALDI mass spectrum of the as-synthesized $Ag_{55}(PET)_{31}$ cluster. Clustering of the molecular ion is seen.

nearest to the cluster core (marked 1 in inset of Fig. 3A). Similarly, the peak at 2870 cm^{-1} also shows a shift (but here it is a blue shift) which might be because of the other C–H bond on the same carbon, closer to the cluster core. In the C–H bending region, two peaks at 1380 cm^{-1} and 1363 cm^{-1} in free thiol merge with each other giving rise to a single broad peak while forming the cluster, which could be attributed to the C–H bend of the nearest carbon (marked 1 in inset of Fig. 3A). Small angle X-ray scattering (SAXS) suggest the high monodispersity of the cluster (Fig. 4A and B) and the average particle size was found to be 1.796 nm (more details are given in ESI 1†).

Synthesis was optimized to yield a 2-phenylethane thiolate (PET) protected Ag_{55} cluster, which suggests the universality of the synthetic strategy and proposes the feasibility of stabilizing this cluster core with other ligands. UV/Vis spectra show (Fig. 4C) similar bands as presented for the BBS-protected Ag_{55} cluster. The peak at m/z 10.2 kDa in MALDI MS (inset of Fig. 4C) using DCTB as a matrix confirms the formation of $Ag_{55}(PET)_{31}$.[41] Here we could see the dimer and trimer also at respective m/z values, similar to the case of ~Ag_{75} cluster.[42]

Conclusions

In summary, we have successfully synthesized Ag_{55} clusters protected with BBS and PET ligands through a solid state route. Solvent selective extraction and a MeOH induced precipitation technique yields the cluster. From the ESI MS and MALDI MS data, the compositions, $Ag_{55}(BBS)_{31}$ and $Ag_{55}(PET)_{31}$ were confirmed. TGA and SEM/EDAX further supported the composition. Extensive characterization was done to know the cluster system in detail. The PET protected Ag_{55} cluster was prepared to check the adaptability of the cluster core to other ligands. We believe that $Ag_{55}(BBS)_{31}$ and other much sought after stable clusters in organic environments will expose new directions in cluster research, in both experiment and theory. Work towards crystallization is underway.

Acknowledgements

We thank the Department of Science and Technology, Government of India for constantly supporting our research program on nanomaterials. I. C. thanks IITM for a research fellowship.

Notes and references

1 R. Jin, *Nanoscale*, 2010, **2**, 343–362.
2 L. M. Liz-Marzán, *Langmuir*, 2005, **22**, 32–41.
3 J. Zheng, P. R. Nicovich and R. M. Dickson, *Annu. Rev. Phys. Chem.*, 2007, **58**, 409–431.
4 I. Chakraborty, T. Udayabhaskararao and T. Pradeep, *J. Hazard. Mater.*, 2012, **211**, 396–403.
5 H. Wei, Z. Wang, L. Yang, S. Tian, C. Hou and Y. Lu, *Analyst*, 2010, **135**, 1406–1410.
6 I. Chakraborty, S. Bag, U. Landman and T. Pradeep, *J. Phys. Chem. Lett.*, 2013, **4**, 2769–2773.
7 H. Tsunoyama, H. Sakurai, N. Ichikuni, Y. Negishi and T. Tsukuda, *Langmuir*, 2004, **20**, 11293–11296.
8 H. Tsunoyama, H. Sakurai, Y. Negishi and T. Tsukuda, *J. Am. Chem. Soc.*, 2005, **127**, 9374–9375.
9 I. Chakraborty, T. Udayabhaskararao, G. Deepesh and T. Pradeep, *J. Mater. Chem. B*, 2013, **1**, 4059–4064.
10 T. Chen, S. Xu, T. Zhao, L. Zhu, D. Wei, Y. Li, H. Zhang and C. Zhao, *ACS Appl. Mater. Interfaces*, 2012, **4**, 5766–5774.
11 C. E. Briant, B. R. C. Theobald, J. W. White, L. K. Bell, D. M. P. Mingos and A. J. Welch, *J. Chem. Soc., Chem. Commun.*, 1981, 201–202.
12 G. Schmid, R. Pfeil, R. Boese, F. Bandermann, S. Meyer, G. H. M. Calis and J. W. A. van der Velden, *Chem. Ber.*, 1981, **114**, 3634–3642.
13 K. Nunokawa, S. Onaka, M. Ito, M. Horibe, T. Yonezawa, H. Nishihara, T. Ozeki, H. Chiba, S. Watase and M. Nakamoto, *J. Organomet. Chem.*, 2006, **691**, 638–642.
14 M. W. Heaven, A. Dass, P. S. White, K. M. Holt and R. W. Murray, *J. Am. Chem. Soc.*, 2008, **130**, 3754–3755.
15 Y. Negishi, K. Nobusada and T. Tsukuda, *J. Am. Chem. Soc.*, 2005, **127**, 5261–5270.
16 P. D. Jadzinsky, G. Calero, C. J. Ackerson, D. A. Bushnell and R. D. Kornberg, *Science*, 2007, **318**, 430–433.
17 G. Schmid, *Chem. Soc. Rev.*, 2008, **37**, 1909–1930.
18 G. Schmid, W. Meyer-Zaika, R. Pugin, T. Sawitowski, J.-P. Majoral, A.-M. Caminade and C.-O. Turrin, *Chem.–Eur. J.*, 2000, **6**, 1693–1697.
19 G. Schmid, R. Pugin, T. Sawitowski, U. Simon and B. Marler, *Chem. Commun.*, 1999, 1303–1304.
20 L. F. Chi, M. Hartig, T. Drechsler, T. Schwaack, C. Seidel, H. Fuchs and G. Schmid, *Appl. Phys. A: Mater. Sci. Process.*, 1998, **66**, S187–S190.
21 Y. Liu, W. Meyer-Zaika, S. Franzka, G. Schmid, M. Tsoli and H. Kuhn, *Angew. Chem., Int. Ed.*, 2003, **42**, 2853–2857.
22 H. Tsunoyama, Y. Negishi and T. Tsukuda, *J. Am. Chem. Soc.*, 2006, **128**, 6036–6037.
23 H. Tsunoyama, P. Nickut, Y. Negishi, K. Al-Shamery, Y. Matsumoto and T. Tsukuda, *J. Phys. Chem. C*, 2007, **111**, 4153–4158.
24 R. Tsunoyama, H. Tsunoyama, P. Pannopard, J. Limtrakul and T. Tsukuda, *J. Phys. Chem. C*, 2010, **114**, 16004–16009.
25 H. Qian and R. Jin, *Chem. Commun.*, 2011, **47**, 11462–11464.
26 Z. Wu, E. Lanni, W. Chen, M. E. Bier, D. Ly and R. Jin, *J. Am. Chem. Soc.*, 2009, **131**, 16672–16674.
27 T. U. B. Rao and T. Pradeep, *Angew. Chem., Int. Ed.*, 2010, **49**, 3925–3929.
28 T. U. B. Rao, B. Nataraju and T. Pradeep, *J. Am. Chem. Soc.*, 2010, **132**, 16304–16307.
29 I. Chakraborty, W. Kurashige, K. Kanehira, L. Gell, H. Häkkinen, Y. Negishi and T. Pradeep, *J. Phys. Chem. Lett.*, 2013, **4**, 3351–3355.
30 K. M. Harkness, Y. Tang, A. Dass, J. Pan, N. Kothalawala, V. J. Reddy, D. E. Cliffel, B. Demeler, F. Stellacci, O. M. Bakr and J. A. McLean, *Nanoscale*, 2012, **4**, 4269–4274.
31 M. R. Branham, A. D. Douglas, A. J. Mills, J. B. Tracy, P. S. White and R. W. Murray, *Langmuir*, 2006, **22**, 11376–11383.
32 I. Chakraborty, A. Govindarajan, J. Erusappan, A. Ghosh, T. Pradeep, B. Yoon, R. L. Whetten and U. Landman, *Nano Lett.*, 2012, **12**, 5861–5866.
33 Y. Negishi, R. Arai, Y. Niihori and T. Tsukuda, *Chem. Commun.*, 2011, **47**, 5693–5695.
34 H. Yang, J. Lei, B. Wu, Y. Wang, M. Zhou, A. Xia, L. Zheng and N. Zheng, *Chem. Commun.*, 2013, **49**, 300–302.
35 H. Yang, Y. Wang and N. Zheng, *Nanoscale*, 2013, **5**, 2674–2677.
36 A. Desireddy, B. E. Conn, J. Guo, B. Yoon, R. N. Barnett, B. M. Monahan, K. Kirschbaum, W. P. Griffith, R. L. Whetten, U. Landman and T. P. Bigioni, *Nature*, 2013, **501**, 399–402.
37 H. Yang, Y. Wang, H. Huang, L. Gell, L. Lehtovaara, S. Malola, H. Häkkinen and N. Zheng, *Nat. Commun.*, 2013, **4**, 2422.
38 Z. Luo, V. Nachammai, B. Zhang, N. Yan, D. T. Leong, D.-e. Jiang and J. Xie, *J. Am. Chem. Soc.*, 2014, **136**, 10577–10580.
39 Y. Yu, X. Chen, Q. Yao, Y. Yu, N. Yan and J. Xie, *Chem. Mater.*, 2013, **25**, 946–952.
40 X. Yuan, B. Zhang, Z. Luo, Q. Yao, D. T. Leong, N. Yan and J. Xie, *Angew. Chem., Int. Ed.*, 2014, **53**, 4623–4627.
41 I. Chakraborty, J. Erusappan, A. Govindarajan, K. S. Sugi, T. Udayabhaskararao, A. Ghosh and T. Pradeep, *Nanoscale*, 2014, **6**, 8024–8031.
42 I. Chakraborty, T. Udayabhaskararao and T. Pradeep, *Chem. Commun.*, 2012, **48**, 6788–6790.
43 T. Udayabhaskararao and T. Pradeep, *J. Phys. Chem. Lett.*, 2013, 1553–1564.
44 H. Qian, Y. Zhu and R. Jin, *Proc. Natl. Acad. Sci. U. S. A.*, 2012, **109**, 696–700.
45 K. P. Remya, T. Udayabhaskararao and T. Pradeep, *J. Phys. Chem. C*, 2012, **116**, 26019–26026.
46 M. S. Bootharaju and T. Pradeep, *J. Phys. Chem. C*, 2010, **114**, 8328–8336.